Image Similarity Based on Intensity Scaling

Stephen L. Keeling*

Abstract. An image similarity measure based upon intensity scaling is investigated for the registration of images which differ in contast. The measure is introduced for both optical flow and for finite displacements, and registration by the optical flow formulation is found to be independent of image order. While other morphological image matching methods involve differential formulations, the present work simply involves composition with scaling functions. Such rescaling is additionally found to have a smoothing effect on noisy images. Results obtained by Tikhonov regularization of scaling functions are superior to those obtained by a restricted set of basis functions. Computational results are performed for simple test cases as well as for realistic examples taken from magnetic resonance imaging. It is found that the computational cost for the implementation of scaling functions is very small, and yet the resulting image similarity can provide a match between images with smaller errors than that obtained by a sum of squared differences alone. In particular, images which are morphologically equivalent but which are scaled differently and even have different noise levels can be well matched with the scaling functions approach while the sum of squared differences would be unsuitable. In addition, matching is improved for image pairs in which contrast agent or an intensity modulation appears in one image and not in the other.

Keywords: image similarity, scaling functions, intensity modulation, optical flow, finite displacements, Tikhonov regularization, magnetic resonance imaging.

1 Introduction

In this work an image similarity measure based upon scaled intensities, or contrast modulation, is proposed and investigated for the registration of images which differ in contrast. The need for such intensity scaling may result from hard-to-control variations among separate measurements or also from inherent differences between measurement modalities. Specific examples include the scaling drift which often accompanies sequential measurements, the intensity modulation which results from using small magnetic resonance coils as opposed to large body coils [11], and the intensity differences which result from measuring a given tissue by magnetic resonance versus computer tomography.

While image similarity measures are often based upon statistical [16] or mutual information [12], the use of higher order entropies employing probabilities of neighboring pixel pairs [14] demonstrates that local spatial information is advantageous. The simplest measure based upon local information is the sum of squared intensity differences, which is natural when images are related by a simple misalignment. It was recognized in [16] that the correlation coefficient is an ideal image similarity measure when the given images are related by a linear rescaling, but in the present work the scaling functions vary within a function space. In [4] Gauss maps are used to perform morphological, i.e., contrast invariant, image matching. Image level sets are also matched in [3] by using a Mumford-Shah formulation for registration. Higher order derivatives of the optical flow equation residual are penalized for an image similarity measure in [17] to obtain optical flows which do not require image structures to maintain a temporally constant brightness. In [2], the optical flow equation residual is replaced by a contrast invariant similarity measure which aligns level sets, and the optical flow is regularized to be piecewise affine over image segments. While all these image similarity measures involve differential formulations to circumvent the constant brightness assumption, the present work simply involves composition with scaling functions. Such rescaling is even found to have a smoothing effect on noisy images.

*Institut für Mathematik und Wissenschaftliches Rechnen, Karl-Franzens-Universität Graz, Heinrichstraße 36, 8010 Graz, Austria; email: stephen.keeling@uni-graz.at; tel: +43–316–380–5156; fax: +43–316–380–9815.

In order to investigate intensity scaling in relation to different registration models, the similarity measure is built into an optical flow model and into a finite displacement model; see [9] and [10] for the precursors of these constructions without scaling functions. As discussed in [9] in relation to the diffusion model of registration [15], an image registration is more natural when it is independent of image order. This goal is achieved in [9] and [10] for optical flow but found in [10] to be generally unrealizable for finite displacements. Similarly, it is found here that scaling functions may be incorporated into the optical flow model while maintaining the independence of image order. However, for finite displacements the registration result is independent of image order only under special conditions.

The paper can be summarized as follows. First, an image similarity measure based upon intensity scaling is introduced for both optical flow and for finite displacements in Section 2. These similarity measures are incorporated into the respective registration frameworks in Section 3. The optimality conditions and other details from [9] and [10] are reviewed and expanded in Section 3, while the optimality conditions for unregularized scaling functions are derived in Section 4. Regularization of the scaling functions is considered in Section 5 in a continuum and in a discrete setting. Specifically, it is found that results obtained by Tikhonov regularization of scaling functions are superior to those obtained by a restricted set of basis functions. At the end of Section 4, the registration schemes for finite displacements and for optical flow which incorporate scaling functions are summarized algorithmically. Finally, computational results are shown in Section 6 for simple test cases as well as for realistic examples taken from magnetic resonance imaging. It is found that the computational cost for the implementation of scaling functions is very small, and yet the resulting image similarity can provide a match between images with smaller errors than that obtained by a sum of squared differences alone. In particular, images which are morphologically equivalent but which are scaled differently and even have different noise levels can be well matched with the scaling functions approach while the sum of squared differences would be unsuitable. In addition, matching is improved for image pairs in which contrast agent or an intensity modulation appears in one image and not in the other.

2 Similarity Measures

Following the illustration in Fig. 1 for 2D images, let two given images I_0 and I_1 be situated

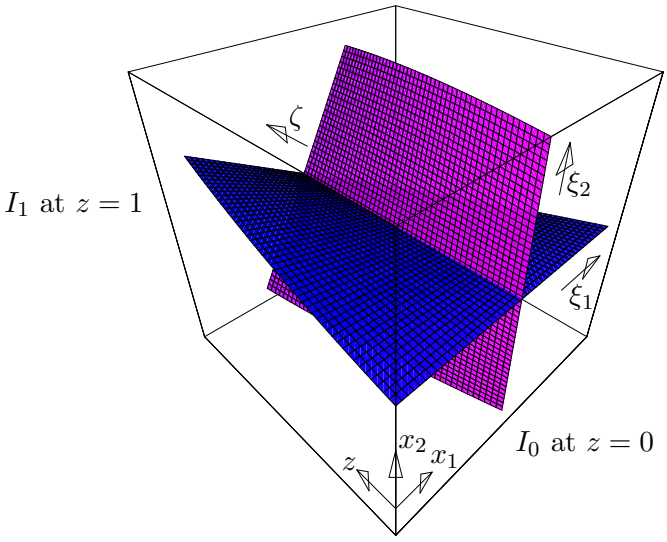

Figure 1: The domain Q with 2D images I_0 and I_1 on the front and back faces Ω_0 and Ω_1, respectively. Curvilinear coordinates are defined to be constant on trajectories connecting like points in I_0 and I_1.

respectively on the front and back faces of a box $Q = \Omega \times (0, 1)$ where a generic cross section of Q is denoted by $\Omega = (0, 1)^N$. In particular, the front and back faces of Q are denoted by Ω_0

and Ω_1, on which I_0 and I_1 are situated respectively. The rectangular spatial coordinates in Ω are denoted by $\boldsymbol{x} = (x_1, \ldots, x_N)$ and the depth or temporal coordinate by z.

The surfaces shown in Fig. 1 are surfaces in which all but one of the curvilinear coordinates $\boldsymbol{\xi} = (\xi_1, \ldots, \xi_N)$ are constant, and the intersection of these surfaces represents a trajectory through Q connecting like points in I_0 and I_1. The coordinates $\boldsymbol{\xi}(\boldsymbol{x}, z)$ are initialized in Ω_0 so that $\boldsymbol{\xi}(\boldsymbol{x}, 0) = \boldsymbol{x}$ holds, and therefore the displacement vector within Q is $\boldsymbol{d}(\boldsymbol{x}, z) = \boldsymbol{x} - \boldsymbol{\xi}(\boldsymbol{x}, z)$. The curvilinear coordinate system is completed by parameterizing a trajectory in the depth direction according to $\zeta = z$. Thus, a trajectory emanating from the point $\boldsymbol{\xi} \in \Omega_0$ is denoted by $\boldsymbol{x}(\boldsymbol{\xi}, \zeta)$. Further, a trajectory tangent is given by $(u_1, \ldots, u_N, 1)$ in terms of the optical flow defined as $\boldsymbol{u} = (u_1, \ldots, u_N) = \boldsymbol{x}_\zeta$. As explained in [10], it is assumed in the present work that the optical flow is autonomous, $\boldsymbol{u}_z = 0$. In the context of finite displacements, the coordinates in Ω_1 corresponding to coordinates $\boldsymbol{\xi}$ in Ω_0 are written as $\boldsymbol{x}(\boldsymbol{\xi}) = \boldsymbol{x}(\boldsymbol{\xi}, 1)$.

In order that every point in Q be situated on some trajectory, it is necessary to consider not only those trajectories emanating from Ω_0 but also those emanating from Ω_1. For this, define curvilinear coordinates $\boldsymbol{\eta} = (\eta_1, \ldots, \eta_N)$ which are also constant along trajectories, but which are initialized in Ω_1 according to $\boldsymbol{\eta}(\boldsymbol{y}, 1) = \boldsymbol{y}$, where $\boldsymbol{y} = (y_1, \ldots, y_N)$ also denotes rectangular spatial coordinates in Ω. Thus, the displacement vector within Q is $\boldsymbol{d}(\boldsymbol{y}, z) = \boldsymbol{y} - \boldsymbol{\eta}(\boldsymbol{y}, z)$, and a trajectory emanating from the point $\boldsymbol{\eta} \in \Omega_1$ is denoted by $\boldsymbol{y}(\boldsymbol{\eta}, \zeta)$. In the context of finite displacements, the coordinates in Ω_0 corresponding to coordinates $\boldsymbol{\eta}$ in Ω_1 are written as $\boldsymbol{y}(\boldsymbol{\eta}) = \boldsymbol{y}(\boldsymbol{\eta}, 0)$.

Since it is not assumed that every point in Ω_0 finds a like point in Ω_1, let the subsets of Ω_0 and Ω_1 with respect to which trajectories extend completely through the full depth of Q be denoted respectively by $\Omega_0^{\mathrm{c}} = \{\boldsymbol{\xi} \in \Omega_0 : \boldsymbol{x}(\boldsymbol{\xi}, \zeta) \in Q, 0 < \zeta < 1\}$ and $\Omega_1^{\mathrm{c}} = \{\boldsymbol{\eta} \in \Omega_1 : \boldsymbol{y}(\boldsymbol{\eta}, \zeta) \in Q, 0 < \zeta < 1\}$. For those trajectories extending incompletely through Q define $\Omega_0^{\mathrm{i}} = \Omega_0 \backslash \Omega_0^{\mathrm{c}}$ and $\Omega_1^{\mathrm{i}} = \Omega_0 \backslash \Omega_1^{\mathrm{c}}$.

2.1 Similarity for Finite Displacements without Scaling

A similarity measure is to be defined here involving at least the squared differences $[I_0(\boldsymbol{\xi}) - I_1(\boldsymbol{x}(\boldsymbol{\xi}))]^2$ over Ω_0^{c}. However, as discussed in detail in [10], Ω_0^{c} depends upon $\boldsymbol{x}(\boldsymbol{\xi})$. To avoid having to differentiate the domain with respect to the displacement for optimization, it is assumed that the images I_0 and I_1 can be continued in $\boldsymbol{R}^N$ by their respective *background* intensities, I_0^∞ and I_1^∞, which are understood as those intensities for which no active signal is measured. With such continuations, $[I_0(\boldsymbol{\xi}) - I_1(\boldsymbol{x}(\boldsymbol{\xi}))]^2$ can be considered for $\boldsymbol{\xi} \in \boldsymbol{R}^N$. To restrict the resulting similarity measure to ∂Q, the sum of squared differences can be considered without intensity scaling as follows:

$$\begin{aligned} &\int_{\Omega_0^{\mathrm{c}}} \left[I_0(\boldsymbol{\xi}) - I_1(\boldsymbol{x}(\boldsymbol{\xi}))\right]^2 d\boldsymbol{\xi} + \int_{\Omega_1^{\mathrm{c}}} \left[I_0(\boldsymbol{y}(\boldsymbol{\eta})) - I_1(\boldsymbol{\eta})\right]^2 d\boldsymbol{\eta} \\ &\quad + \int_{\Omega_0^{\mathrm{i}}} \left[I_0(\boldsymbol{\xi}) - I_1^\infty\right]^2 d\boldsymbol{\xi} + \int_{\Omega_1^{\mathrm{i}}} \left[I_0^\infty - I_1(\boldsymbol{\eta})\right]^2 d\boldsymbol{\eta} \end{aligned} \tag{2.1}$$

where the background intensities are used as though the side of the box Q,

$$\Gamma = \partial Q \backslash \{\Omega_0 \cup \Omega_1\} \tag{2.2}$$

were not present and the displacements impinging upon Γ from Ω_1 or Ω_0 would respectively be connected with I_0 and I_1 continued in $\boldsymbol{R}^N$ by their background intensities.

2.2 Similarity for Finite Displacements with Scaling

Intensity scaling can be introduced as follows to the similarity measure (2.1). Let $\sigma_0 : [0,1] \to [0,1]$ and $\sigma_1 : [0,1] \to [0,1]$ be functions scaling the intensities of I_0 and I_1 respectively.

Then an image similarity measure with intensity scaling is given for finite displacements by modifying (2.1) according to:

$$\begin{aligned}&\mathcal{S}_{\mathrm{fd}}(\boldsymbol{x},\sigma_0,\sigma_1)\\&=\int_{\Omega_0^{\mathrm{c}}}\left[\sigma_0(I_0(\boldsymbol{\xi}))-I_1(\boldsymbol{x}(\boldsymbol{\xi}))\right]^2 d\boldsymbol{\xi}+\int_{\Omega_0^{\mathrm{i}}}\left[\sigma_0(I_0(\boldsymbol{\xi}))-I_1^{\infty}\right]^2 d\boldsymbol{\xi}+\int_{\Omega_1^{\mathrm{i}}}\left[\sigma_0(I_0^{\infty})-I_1(\boldsymbol{\eta})\right]^2 d\boldsymbol{\eta}\\&+\int_{\Omega_1^{\mathrm{c}}}\left[I_0(\boldsymbol{y}(\boldsymbol{\eta}))-\sigma_1(I_1(\boldsymbol{\eta}))\right]^2 d\boldsymbol{\eta}+\int_{\Omega_0^{\mathrm{i}}}\left[I_0(\boldsymbol{\xi})-\sigma_1(I_1^{\infty})\right]^2 d\boldsymbol{\xi}+\int_{\Omega_1^{\mathrm{i}}}\left[I_0^{\infty}-\sigma_1(I_1(\boldsymbol{\eta}))\right]^2 d\boldsymbol{\eta}\end{aligned}\tag{2.3}$$

where each line in (2.3) represents the effect of scaling just one of the given images. As shown in Section 3, reciprocal scaling must be performed in order that the registration be independent of image order. Nevertheless, reciprocity can be achieved for finite displacements only under limited circumstances, while reciprocity can be achieved in general for optical flow.

2.3 Similarity for Optical Flow without Scaling

By regarding the displacements in (2.1) as the endpoints of trajectories in Q, the measure (2.1) is equivalent to the following,

$$\int_{\Omega_0^{\mathrm{c}}}\int_0^1\left[\frac{dI}{d\zeta}\right]^2 d\zeta d\boldsymbol{\xi}+\int_{\Omega_0^{\mathrm{i}}}\int_0^{\acute{\zeta}(\boldsymbol{\xi})}\left[\frac{dI}{d\zeta}\right]^2 d\zeta d\boldsymbol{\xi}+\int_{\Omega_1^{\mathrm{i}}}\int_{\grave{\zeta}(\boldsymbol{\eta})}^1\left[\frac{dI}{d\zeta}\right]^2 d\zeta d\boldsymbol{\eta}\tag{2.4}$$

under the constraints [9]:

$$I(\boldsymbol{\xi},0)=I_0(\boldsymbol{\xi}),\quad I(\boldsymbol{x}(\boldsymbol{\xi},1),1)=I_1(\boldsymbol{x}(\boldsymbol{\xi},1)),\quad \boldsymbol{\xi}\in\Omega_0^{\mathrm{c}}\tag{2.5}$$

and

$$I(\boldsymbol{x}(\boldsymbol{\xi},\acute{\zeta}),\acute{\zeta})=I_1^{\infty},\quad \boldsymbol{x}(\boldsymbol{\xi},\acute{\zeta})\in\Gamma,\qquad I(\boldsymbol{y}(\boldsymbol{\eta},\grave{\zeta}),\grave{\zeta})=I_0^{\infty},\quad \boldsymbol{y}(\boldsymbol{\eta},\grave{\zeta})\in\Gamma\tag{2.6}$$

where $\acute{\zeta}$ and $\grave{\zeta}$, as illustrated in Fig. 2, denote the ζ coordinates at which trajectories emanating

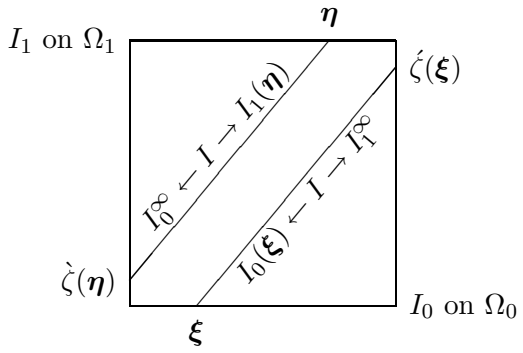

Figure 2: $\acute{\zeta}(\boldsymbol{\xi})$ and $\grave{\zeta}(\boldsymbol{\eta})$ denote the ζ coordinates at which trajectories emanating respectively from $\boldsymbol{\xi}\in\Omega_0^{\mathrm{i}}$ and $\boldsymbol{\eta}\in\Omega_1^{\mathrm{i}}$ meet Γ.

respectively from Ω_0^{i} and Ω_1^{i} meet Γ. Thus, $\acute{\zeta}=\acute{\zeta}(\boldsymbol{\xi})$ and $\grave{\zeta}=\grave{\zeta}(\boldsymbol{\eta})$ are respectively defined implicitly as functions of $\boldsymbol{\xi}\in\Omega_0^{\mathrm{i}}$ and $\boldsymbol{\eta}\in\Omega_1^{\mathrm{i}}$ for (2.4).

A similarity measure which involves infinitesimal instead of finite displacements is obtained by expressing the derivative $dI/d\zeta$ in (2.4) in terms of rectangular coordinates:

$$\frac{dI}{d\zeta}(\boldsymbol{x}(\boldsymbol{\xi},\zeta),\zeta)=\nabla_{\boldsymbol{x}}I\cdot\boldsymbol{x}_{\zeta}+I_{\zeta}=\nabla_{\boldsymbol{x}}I\cdot\boldsymbol{u}+I_z\tag{2.7}$$

to arrive at the following penalty on the optical flow equation residual [8], after neglecting the transformation Jacobian $1/\det[\nabla_{\boldsymbol{\xi}}\boldsymbol{x}]$:

$$\int_Q\left[\nabla_{\boldsymbol{x}}I\cdot\boldsymbol{u}+I_z\right]^2 d\boldsymbol{x}dz.\tag{2.8}$$

This integral is the *Eulerian* counterpart to the *Lagrangian* form appearing in (2.4) [9]. Furthermore, the counterpart to (2.5) in the Eulerian context is given by:

$$I = I_0 \text{ on } \Omega_0, \qquad I = I_1 \text{ on } \Omega_1. \tag{2.9}$$

By defining the outflow and inflow portions respectively of Γ,

$$\Gamma_+ = \{(\boldsymbol{x}, z) \in \partial Q : \boldsymbol{u}^{\mathrm{T}}\boldsymbol{n} > 0\}, \quad \Gamma_- = \{(\boldsymbol{x}, z) \in \partial Q : \boldsymbol{u}^{\mathrm{T}}\boldsymbol{n} < 0\} \tag{2.10}$$

the counterpart to (2.6) in the Eulerian context is given by:

$$I = I_1^{\infty} \text{ on } \Gamma_+, \quad I = I_0^{\infty} \text{ on } \Gamma_-. \tag{2.11}$$

Thus, an image similarity measure without intensity scaling is given for optical flow by (2.8) under the constraints (2.9) and (2.11).

2.4 Similarity for Optical Flow with Scaling

An image similarity measure with reciprocal intensity scaling is given for optical flow by:

$$\mathcal{S}_{\mathrm{of}}(\boldsymbol{u}, I^{(0)}, I^{(1)}, \sigma_0, \sigma_1) = \int_Q \left\{ [\nabla_{\boldsymbol{x}} I^{(0)} \cdot \boldsymbol{u} + I_z^{(0)}]^2 + [\nabla_{\boldsymbol{x}} I^{(1)} \cdot \boldsymbol{u} + I_z^{(1)}]^2 \right\} d\boldsymbol{x} dz \tag{2.12}$$

where the intensity $I^{(0)}$ is constrained by the following modifications of (2.9) and (2.11):

$$I^{(0)} = I_0 \text{ on } \Omega_0, \quad I^{(0)} = \sigma_1(I_1) \text{ on } \Omega_1, \quad I^{(0)} = \sigma_1(I_1^{\infty}) \text{ on } \Gamma_+, \quad I^{(0)} = I_0^{\infty} \text{ on } \Gamma_- \tag{2.13}$$

in which only I_1 is scaled, and the intensity $I^{(1)}$ is constrained by the following modifications of (2.9) and (2.11):

$$I^{(1)} = \sigma_0(I_0) \text{ on } \Omega_0, \quad I^{(1)} = I_1 \text{ on } \Omega_1, \quad I^{(1)} = I_1^{\infty} \text{ on } \Gamma_+, \quad I^{(1)} = \sigma_0(I_0^{\infty}) \text{ on } \Gamma_- \tag{2.14}$$

in which only I_0 is scaled.

3 Registration Formulation and Review

In this section, cost functionals J_{fd} and J_{of} are given for registration respectively with finite displacements and with optical flow. The necessary optimality conditions for the scaling functions in J_{fd} and J_{of} are given in Section 4. The necessary optimality conditions for the remaining variables are discussed in [9] and [10] and are summarized and expanded here in the present context. Note that the regularization models for finite displacements and for optical flow are chosen here, as in [9] and [10], independently from scaling functions, and the formulations are generalized here to include scaling functions. As discussed in detail in Section 5, the intent is to solve the optimality system cyclically for one variable while the others are held fixed.

3.1 Formulation for Finite Displacements

Image registration is achieved by means of a finite displacement field $\boldsymbol{x}(\boldsymbol{\xi})$ by minimizing [10]:

$$J_{\mathrm{fd}}(\boldsymbol{x}, \sigma_0, \sigma_1) = \mathcal{S}_{\mathrm{fd}}(\boldsymbol{x}, \sigma_0, \sigma_1) + \mathcal{R}_{\mathrm{fd}}(\boldsymbol{x}) \tag{3.1}$$

where the similarity measure $\mathcal{S}_{\mathrm{fd}}$ is given in (2.3) and the regularity measure $\mathcal{R}_{\mathrm{fd}}$ is defined by:

$$\mathcal{R}_{\mathrm{fd}}(\boldsymbol{x}) = \mu \sum_{|\alpha|=2} \frac{2!}{\alpha!} \int_{\Omega_0} |\partial_{\boldsymbol{\xi}}^{\alpha} \boldsymbol{x}|^2 d\boldsymbol{\xi}. \tag{3.2}$$

Here $2!/\alpha!$ is the multinomial coefficient for a multi-index α, and the second-order regularity measure $\mathcal{R}_{\rm fd}$ under natural boundary conditions provides *generalized affine registration* in the sense that an affine transformation is obtained when one agrees with the given data [10]. Note that in order for $J_{\rm rd}$ to be defined with the same symmetry as $\mathcal{S}_{\rm fd}$, an additional term $\mathcal{R}_{\rm fd}(\boldsymbol{y})$ penalizing $\boldsymbol{y} = \boldsymbol{x}^{-1}$ over Ω_1 exactly as $\boldsymbol{x}$ is penalized over Ω_0 in $\mathcal{R}_{\rm fd}(\boldsymbol{x})$ may be added to $J_{\rm fd}$ with considerable cost in complexity of the formulation. In connection with (3.2), see also [6] and [13] for curvature based registration and [7] for multigrid approaches to such high-order regularization for registration.

The cost $J_{\rm fd}$ is stationary in the displacement $\boldsymbol{x}$ for fixed σ_0 and σ_1 when $\boldsymbol{x}$ satisfies:

$$B_{\rm fd}(\boldsymbol{x}, \bar{\boldsymbol{x}}) = F_{\rm fd}(\boldsymbol{x}, \bar{\boldsymbol{x}}), \quad \forall \bar{x} \in H^2(\Omega) \tag{3.3}$$

where $H^m(\Omega)$ denotes the usual Sobolev space of functions with distributional derivatives up to order m in $L^2(\Omega)$ [1], and $B_{\rm fd}$ and $F_{\rm fd}$ are defined by [10]:

$$\begin{aligned} B_{\rm fd}(\boldsymbol{x}, \bar{\boldsymbol{x}}) &= \mu \sum_{|\alpha|=2} \frac{2!}{\alpha!} \int_{\Omega_0} [\partial^\alpha_{\boldsymbol{\xi}} \boldsymbol{x}] \cdot [\partial^\alpha_{\boldsymbol{\xi}} \bar{\boldsymbol{x}}] d\boldsymbol{\xi} \qquad (3.4) \\ F_{\rm fd}(\boldsymbol{x}, \bar{\boldsymbol{x}}) &= \int_{\Omega_0^{\rm c}} [\sigma_0(I_0(\boldsymbol{\xi})) - I_1(\boldsymbol{x}(\boldsymbol{\xi}))] \, \nabla_{\boldsymbol{x}} I_1(\boldsymbol{x}(\boldsymbol{\xi}))^{\rm T} \bar{\boldsymbol{x}}(\boldsymbol{\xi}) d\boldsymbol{\xi} \\ &+ \int_{\Omega_1^{\rm c}} [I_0(\boldsymbol{y}(\boldsymbol{\eta})) - \sigma_1(I_1(\boldsymbol{\eta}))] \nabla_{\boldsymbol{y}} I_0(\boldsymbol{y}(\boldsymbol{\eta}))^{\rm T} \nabla_{\boldsymbol{\eta}} \boldsymbol{y}(\boldsymbol{\eta}) \bar{\boldsymbol{x}}(\boldsymbol{y}(\boldsymbol{\eta})) d\boldsymbol{\eta}. \end{aligned}$$

The solvability of systems associated with a quasi-Newton iteration for (3.3) is established in [10].

3.2 Formulation for Optical Flow

Image registration as well as interpolation are achieved by means of autonomous optical flow by minimizing [10]:

$$J_{\rm of}(\boldsymbol{u}, I^{(0)}, I^{(1)}, \sigma_0, \sigma_1) = \mathcal{S}_{\rm of}(\boldsymbol{u}, I^{(0)}, I^{(1)}, \sigma_0, \sigma_1) + \mathcal{R}_{\rm of}(\boldsymbol{u}) \tag{3.5}$$

subject to (2.13) and (2.14), where the similarity measure $\mathcal{S}_{\rm of}$ is given in (2.12) and the regularity measure $\mathcal{R}_{\rm of}$ is defined by:

$$\mathcal{R}_{\rm of}(\boldsymbol{u}) = \mu \int_\Omega |\nabla \boldsymbol{u}^{\rm T} + \nabla \boldsymbol{u}|^2 d\boldsymbol{x}. \tag{3.6}$$

Here $|\nabla \boldsymbol{u}|^2 = \nabla \boldsymbol{u} : \nabla \boldsymbol{u}$ and $:$ denotes a componentwise matrix scalar product. Under natural boundary conditions, $\mathcal{R}_{\rm of}$ provides *generalized rigid registration* in the sense that a rigid transformation is obtained when one agrees with the given data [9] [10]. Trajectories through the domain Q are defined by integrating the optical flow under boundary conditions, i.e., by solving:

$$\boldsymbol{x}(\boldsymbol{\xi}, \zeta) = \boldsymbol{\xi} + \int_0^\zeta \boldsymbol{u}(\boldsymbol{x}(\boldsymbol{\xi}, \rho)) d\rho, \quad \boldsymbol{\xi} \in \Omega_0, \quad \zeta \in [0, 1] \tag{3.7}$$

and

$$\boldsymbol{y}(\boldsymbol{\eta}, \zeta) = \boldsymbol{\eta} + \int_\zeta^1 \boldsymbol{u}(\boldsymbol{y}(\boldsymbol{\eta}, \rho)) d\rho, \quad \boldsymbol{\eta} \in \Omega_1, \quad \zeta \in [0, 1]. \tag{3.8}$$

A registration is given by the coordinate transformation $\boldsymbol{x}(\boldsymbol{\xi}, 1)$ and by the inverse transformation $\boldsymbol{y}(\boldsymbol{\eta}, 0)$. The intensity I used below to compute the optical flow in (3.18) is

$$I = [I^{(0)} + I^{(1)}]/2. \tag{3.9}$$

It will be seen that this intensity permits reciprocal scaling and avoids intensity variations, such as in

$$\mathcal{I}(\boldsymbol{x}, z) = (1 - z) I^{(0)}(\boldsymbol{x}, z) + z I^{(1)}(\boldsymbol{x}, z), \tag{3.10}$$

which result only from scaling differences as opposed to misregistration. On the other hand, once the optical flow has been computed, the intensity $\mathcal{I}$ is a more suitable interpolation than I.

As explained in detail in [9], the cost $J_{\rm of}$ is stationary in one of the intensities, say $I^{(0)}$, for fixed $\boldsymbol{u}$, σ_0 and σ_1 when $I^{(0)}$ satisfies:

$$\frac{d^2 I^{(0)}}{d\zeta^2} + (\nabla \cdot \boldsymbol{u}) \frac{dI^{(0)}}{d\zeta} = 0 \tag{3.11}$$

along a trajectory, together with boundary conditions which depend upon the endpoints of the trajectory. Specifically, if the trajectory begins in Ω_0, the boundary conditions for $I^{(0)}$ are:

$$I^{(0)}(\boldsymbol{\xi}, 0) = I_0(\boldsymbol{\xi}) \quad \text{and} \quad \begin{cases} I^{(0)}(\boldsymbol{x}(\boldsymbol{\xi}, 1), 1) = \sigma_1(I_1(\boldsymbol{x}(\boldsymbol{\xi}, 1))), & & \boldsymbol{\xi} \in \Omega_0^{\rm c} \\ I^{(0)}(\boldsymbol{x}(\boldsymbol{\xi}, 1), 1) = \sigma_1(I_1^{\infty}), & \boldsymbol{x}(\boldsymbol{\xi}, \acute{\zeta}) \in \Gamma, & \boldsymbol{\xi} \in \Omega_0^{\rm i} \end{cases} \tag{3.12}$$

In case the trajectory begins in Ω_1, the boundary conditions for $I^{(0)}$ are:

$$I^{(0)}(\boldsymbol{\eta}, 1) = \sigma_1(I_1(\boldsymbol{\eta})) \quad \text{and} \quad \begin{cases} I^{(0)}(\boldsymbol{y}(\boldsymbol{\eta}, 0), 0) = I_0(\boldsymbol{y}(\boldsymbol{\eta}, 0)), & & \boldsymbol{\eta} \in \Omega_1^{\rm c} \\ I^{(0)}(\boldsymbol{y}(\boldsymbol{\eta}, 0), 0) = I_0^{\infty}, & \boldsymbol{y}(\boldsymbol{\eta}, \grave{\zeta}) \in \Gamma, & \boldsymbol{\eta} \in \Omega_1^{\rm i} \end{cases} \tag{3.13}$$

As illustrated in Fig. 2, the parameters $\acute{\zeta}$ and $\grave{\zeta}$ denote the ζ coordinates at which trajectories emanating respectively from $\Omega_0^{\rm i}$ and $\Omega_1^{\rm i}$ meet Γ. For the solution to these boundary value problems along trajectories, define U and V by:

$$U(\boldsymbol{\xi}, \zeta, \acute{\zeta}) = \frac{\tilde{U}(\boldsymbol{\xi}, \zeta) - \tilde{U}(\boldsymbol{\xi}, 0)}{\tilde{U}(\boldsymbol{\xi}, \acute{\zeta}) - \tilde{U}(\boldsymbol{\xi}, 0)}, \qquad \tilde{U}(\boldsymbol{\xi}, \zeta) = \int_{\zeta_0}^{\zeta} \exp\left[- \int_{\zeta_0}^{\varrho} \nabla \cdot \boldsymbol{u}(\boldsymbol{x}(\boldsymbol{\xi}, \rho)) d\rho \right] d\varrho, \tag{3.14}$$

for $\boldsymbol{\xi} \in \Omega_0$, $\zeta \in [0, \acute{\zeta}]$, and arbitrary $\zeta_0 \in [0, \acute{\zeta}]$, and:

$$V(\boldsymbol{\eta}, \grave{\zeta}, \zeta) = \frac{\tilde{V}(\boldsymbol{\eta}, 1) - \tilde{V}(\boldsymbol{\eta}, \zeta)}{\tilde{V}(\boldsymbol{\eta}, 1) - \tilde{V}(\boldsymbol{\eta}, \grave{\zeta})}, \qquad \tilde{V}(\boldsymbol{\eta}, \zeta) = \int_{\zeta_0}^{\zeta} \exp\left[- \int_{\zeta_0}^{\varrho} \nabla \cdot \boldsymbol{u}(\boldsymbol{y}(\boldsymbol{\eta}, \rho)) d\rho \right] d\varrho, \tag{3.15}$$

for $\boldsymbol{\eta} \in \Omega_1$, $\zeta \in [\grave{\zeta}, 1]$, and arbitrary $\zeta_0 \in [\grave{\zeta}, 1]$. Then, $I^{(0)}$ is given in a Lagrangian frame by:

$$I^{(0)}(\boldsymbol{x}(\boldsymbol{\xi}, \zeta), \zeta) = \begin{cases} I_0(\boldsymbol{\xi})[1 - U(\boldsymbol{\xi}, \zeta, 1)] + \sigma_1(I_1(\boldsymbol{x}(\boldsymbol{\xi}, 1)))U(\boldsymbol{\xi}, \zeta, 1), & & \boldsymbol{\xi} \in \Omega_0^{\rm c} \\ I_0(\boldsymbol{\xi})[1 - U(\boldsymbol{\xi}, \zeta, \acute{\zeta})] + \sigma_1(I_1^{\infty})U(\boldsymbol{\xi}, \zeta, \acute{\zeta}), & \boldsymbol{x}(\boldsymbol{\xi}, \acute{\zeta}) \in \Gamma, & \boldsymbol{\xi} \in \Omega_0^{\rm i} \end{cases} \tag{3.16}$$

and:

$$I^{(0)}(\boldsymbol{y}(\boldsymbol{\eta}, \zeta), \zeta) = \begin{cases} \sigma_1(I_1(\boldsymbol{\eta}))[1 - V(\boldsymbol{\eta}, 0, \zeta)] + I_0(\boldsymbol{y}(\boldsymbol{\eta}, 0))V(\boldsymbol{\eta}, 0, \zeta), & & \boldsymbol{\eta} \in \Omega_1^{\rm c} \\ \sigma_1(I_1(\boldsymbol{\eta}))[1 - V(\boldsymbol{\eta}, \grave{\zeta}, \zeta)] + I_0^{\infty}V(\boldsymbol{\eta}, \grave{\zeta}, \zeta), & \boldsymbol{y}(\boldsymbol{\eta}, \grave{\zeta}) \in \Gamma, & \boldsymbol{\eta} \in \Omega_1^{\rm i} \end{cases} \tag{3.17}$$

and $I^{(1)}$ is given similarly by scaling I_0 instead of I_1.

Finally, the cost $J_{\rm of}$ is stationary in the optical flow $\boldsymbol{u}$ for fixed $I^{(0)}$, $I^{(1)}$, σ_0 and σ_1 when $\boldsymbol{u}$ satisfies:

$$B_{\rm of}(\boldsymbol{u}, \bar{\boldsymbol{u}}) = F_{\rm of}(\bar{\boldsymbol{u}}), \quad \forall \boldsymbol{u} \in H^1(\Omega), \tag{3.18}$$

where $B_{\rm of}$ and $F_{\rm of}$ are defined by:

$$B_{\rm of}(\boldsymbol{u}, \bar{\boldsymbol{u}}) = \int_Q (\nabla I \cdot \boldsymbol{u})(\nabla I \cdot \bar{\boldsymbol{u}}) d\boldsymbol{x} dz + \mu \int_\Omega \left(\nabla \boldsymbol{u}^{\rm T} + \nabla \boldsymbol{u} \right) : \left(\nabla \bar{\boldsymbol{u}}^{\rm T} + \nabla \bar{\boldsymbol{u}} \right) d\boldsymbol{x} \tag{3.19}$$

$$F_{\rm of}(\bar{\boldsymbol{u}}) = - \int_Q I_z \nabla I \cdot \bar{\boldsymbol{u}} d\boldsymbol{x} dz. \tag{3.20}$$

Note that no additional boundary conditions are imposed by restricting the domain of these forms, and thus natural boundary conditions hold. The solvability of (3.18) is established in [9].

4 Optimality Conditions for Scaling Functions

In this section the necessary optimality conditions for the scaling functions in J_{fd} and J_{of} are derived. The formulas are given only for σ_0, and the corresponding formulas for σ_1 are obtained similarly.

4.1 Optimality Conditions in Case of Finite Displacements

First consider the differentiation of J_{fd} with respect to the scaling functions for fixed $\boldsymbol{x}$ (and $\boldsymbol{y} = \boldsymbol{x}^{-1}$). Since $\mathcal{R}_{\mathrm{fd}}$ is independent of the scaling functions, $\mathcal{S}_{\mathrm{fd}}$ in (2.3) is used to compute the variational derivative with respect to σ_0 for fixed σ_1:

$$\frac{1}{2}\frac{\delta J_{\mathrm{fd}}}{\delta \sigma_0}(\sigma_0;\bar{\sigma}_0) = \int_{\Omega_0} \left[\sigma_0(I_0(\boldsymbol{\xi})) - \mathcal{I}_1(\boldsymbol{\xi})\right] \bar{\sigma}_0(I_0(\boldsymbol{\xi}))d\boldsymbol{\xi} + \int_{\Omega_1^{\mathrm{i}}} \left[\sigma_0(I_0^\infty) - I_1(\boldsymbol{\eta})\right] \bar{\sigma}_0(I_0^\infty)d\boldsymbol{\eta}. \quad (4.1)$$

where the morphing of I_1 into Ω_0 is given by:

$$\mathcal{I}_1(\boldsymbol{\xi}) = \begin{cases} I_1(\boldsymbol{x}), & \boldsymbol{x} = \boldsymbol{x}(\boldsymbol{\xi}) \text{ or } \boldsymbol{x}(\boldsymbol{\xi},1) \quad \boldsymbol{\xi} \in \Omega_0^{\mathrm{c}} \\ I_1^\infty, & \boldsymbol{\xi} \in \Omega_0^{\mathrm{i}} \end{cases} \quad (4.2)$$

and $\mathcal{I}_0(\boldsymbol{\eta})$ is defined similarly by exchanging the subscripts 0 and 1, the variables $\boldsymbol{\xi}$ and $\boldsymbol{\eta}$, and the transformations $\boldsymbol{x}(\boldsymbol{\xi}), \boldsymbol{x}(\boldsymbol{\xi},1)$ and $\boldsymbol{y}(\boldsymbol{\eta}), \boldsymbol{y}(\boldsymbol{\eta},0)$. Now let $\check{\iota}_0$ and $\hat{\iota}_0$ respectively denote the minimum and maximum values of I_0 over Ω_0, so the range of I_0 is contained in $[\check{\iota}_0, \hat{\iota}_0]$. Then assume that $|\nabla I_0| = 0$ holds only when I_0 assumes values $K_0 \subset [\check{\iota}_0, \hat{\iota}_0]$. Similarly, $\check{\iota}_1$ and $\hat{\iota}_1$ are defined so that the range of I_1 is contained in $[\check{\iota}_1, \hat{\iota}_1]$, and $|\nabla I_1| = 0$ holds when I_1 assumes values $K_1 \subset [\check{\iota}_1, \hat{\iota}_1]$. Now, let the integral in (4.1) be decomposed into the support of $|\nabla I_0|$ and its complement in Ω_0. Under the assumption that the given images are represented by multilinear interpolation of their pixel values, the coarea formula [5] can be used to represent the variational derivative in (4.1) in the following form:

$$\begin{aligned} \frac{\delta J_{\mathrm{fd}}}{\delta \sigma_0}(\sigma_0;\bar{\sigma}_0) &= 2\bar{\sigma}_0(I_0^\infty)\left[\int_{I_0(\boldsymbol{\xi})=I_0^\infty} [\sigma_0(I_0^\infty) - \mathcal{I}_1(\boldsymbol{\xi})]d\boldsymbol{\xi} + \int_{\Omega_1^{\mathrm{i}}} [\sigma_0(I_0^\infty) - I_1(\boldsymbol{\eta})]d\boldsymbol{\eta}\right] \\ &+ 2\sum_{\iota \in K_0 \setminus \{I_0^\infty\}} \bar{\sigma}_0(\iota) \int_{I_0(\boldsymbol{\xi})=\iota} [\sigma_0(\iota) - \mathcal{I}_1(\boldsymbol{\xi})]d\boldsymbol{\xi} \\ &+ 2\int_{\check{\iota}_0}^{\hat{\iota}_0} \bar{\sigma}_0(\iota) \left[\int_{I_0(\boldsymbol{\xi})=\iota, \nabla I_0(\boldsymbol{\xi})\neq 0} \frac{[\sigma_0(\iota) - \mathcal{I}_1(\boldsymbol{\xi})]}{|\nabla I_0(\boldsymbol{\xi})|} d\boldsymbol{\xi}\right] d\iota. \end{aligned} \quad (4.3)$$

Requiring the variational derivative in (4.3) to vanish for all perturbations $\bar{\sigma}_0$ leads to the following optimality condition for σ_0:

$$\sigma_0(\iota) = \begin{cases} \left[\int_{I_0(\boldsymbol{\xi})=\iota} \mathcal{I}_1(\boldsymbol{\xi})d\boldsymbol{\xi} + \int_{\Omega_1^{\mathrm{i}}} I_1(\boldsymbol{\eta})d\boldsymbol{\eta}\right] \Big/ \left[\int_{I_0(\boldsymbol{\xi})=\iota} d\boldsymbol{\xi} + \int_{\Omega_1^{\mathrm{i}}} d\boldsymbol{\eta}\right], & \iota = I_0^\infty \\ \int_{I_0(\boldsymbol{\xi})=\iota} \mathcal{I}_1(\boldsymbol{\xi})d\boldsymbol{\xi} \Big/ \int_{I_0(\boldsymbol{\xi})=\iota} d\boldsymbol{\xi}, & \iota \in K_0 \setminus \{I_0^\infty\} \\ \int_{I_0(\boldsymbol{\xi})=\iota} \frac{\mathcal{I}_1(\boldsymbol{\xi})d\boldsymbol{\xi}}{|\nabla I_0(\boldsymbol{\xi})|} \Big/ \int_{I_0(\boldsymbol{\xi})=\iota} \frac{d\boldsymbol{\xi}}{|\nabla I_0(\boldsymbol{\xi})|}, & \iota \in [\check{\iota}_0, \hat{\iota}_0] \setminus K_0. \end{cases} \quad (4.4)$$

The optimality condition for σ_1 is given similarly by exchanging the subscripts 0 and 1 and the variables $\boldsymbol{\xi}$ and $\boldsymbol{\eta}$.

4.2 Optimality Conditions in Case of Optical Flow

Now consider the differentiation of J_{of} with respect to the scaling functions for fixed I and $\boldsymbol{u}$. For the variational derivative with respect to σ_0, only the $I^{(1)}$ term of $\mathcal{S}_{\text{of}}$ depends upon σ_0, and this term is written in a Lagrangian frame as follows:

$$\begin{aligned}\int_Q [\nabla I^{(1)} \cdot \boldsymbol{u} + I_z^{(1)}]^2 d\boldsymbol{x} dz = \int_{\Omega_0^{\text{c}}} \int_0^1 \left[\frac{dI^{(1)}}{d\zeta}\right]^2 \det\left(\nabla_{\boldsymbol{\xi}} \boldsymbol{x}\right) d\zeta d\boldsymbol{\xi} + \\ \int_{\Omega_0^{\text{i}}} \int_0^{\acute{\zeta}(\boldsymbol{\xi})} \left[\frac{dI^{(1)}}{d\zeta}\right]^2 \det\left(\nabla_{\boldsymbol{\xi}} \boldsymbol{x}\right) d\zeta d\boldsymbol{\xi} + \int_{\Omega_1^{\text{i}}} \int_{\grave{\zeta}(\boldsymbol{\eta})}^1 \left[\frac{dI^{(1)}}{d\zeta}\right]^2 \det\left(\nabla_{\boldsymbol{\eta}} \boldsymbol{y}\right) d\zeta d\boldsymbol{\eta}\end{aligned} \tag{4.5}$$

Also, as explained in relation to Fig. 2, $\acute{\zeta}$ and $\grave{\zeta}$ are defined implicitly as functions of $\boldsymbol{\xi}$ and $\boldsymbol{\eta}$, respectively, and they can be used to express (4.5) explicitly in terms of σ_0 according to:

$$\begin{aligned}&\int_Q [\nabla I^{(1)} \cdot \boldsymbol{u} + I_z^{(1)}]^2 d\boldsymbol{x} dz \\ =\ & \int_{\Omega_0^{\text{c}}} \int_0^1 [\sigma_0(I_0(\boldsymbol{\xi})) - I_1(\boldsymbol{x}(\boldsymbol{\xi},1))]^2 U_\zeta^2(\boldsymbol{\xi},\zeta,1) \det\left(\nabla_{\boldsymbol{\xi}} \boldsymbol{x}\right) d\zeta d\boldsymbol{\xi} \\ +\ & \int_{\Omega_0^{\text{i}}} \int_0^{\acute{\zeta}(\boldsymbol{\xi})} [\sigma_0(I_0(\boldsymbol{\xi})) - I_1^\infty]^2 U_\zeta^2(\boldsymbol{\xi},\zeta,\acute{\zeta}(\boldsymbol{\xi})) \det\left(\nabla_{\boldsymbol{\xi}} \boldsymbol{x}\right) d\zeta d\boldsymbol{\xi} \\ +\ & \int_{\Omega_1^{\text{i}}} \int_{\grave{\zeta}(\boldsymbol{\eta})}^1 [\sigma_0(I_0^\infty) - I_1(\boldsymbol{\eta})]^2 V_\zeta^2(\boldsymbol{\eta},\grave{\zeta}(\boldsymbol{\eta}),\zeta) \det\left(\nabla_{\boldsymbol{\eta}} \boldsymbol{y}\right) d\zeta d\boldsymbol{\eta}.\end{aligned} \tag{4.6}$$

The $I^{(0)}$ term of $\mathcal{S}_{\text{of}}$ can be expressed similarly in terms of σ_1 after writing the first integral in the counterpart to (4.5) equivalently over Ω_1^{c}. To simplify the expressions above, define:

$$\mathcal{U}(\boldsymbol{\xi}) = \begin{cases} \displaystyle\int_0^1 U_\zeta^2(\boldsymbol{\xi},\zeta,1) \det\left(\nabla_{\boldsymbol{\xi}} \boldsymbol{x}\right) d\zeta, & \boldsymbol{\xi} \in \Omega_0^{\text{c}} \\ \displaystyle\int_0^{\acute{\zeta}(\boldsymbol{\xi})} U_\zeta^2(\boldsymbol{\xi},\zeta,\acute{\zeta}(\boldsymbol{\xi})) \det\left(\nabla_{\boldsymbol{\xi}} \boldsymbol{x}\right) d\zeta, & \boldsymbol{\xi} \in \Omega_0^{\text{i}} \end{cases} \tag{4.7}$$

$$\mathcal{V}(\boldsymbol{\eta}) = \begin{cases} \displaystyle\int_0^1 V_\zeta^2(\boldsymbol{\eta},0,\zeta) \det\left(\nabla_{\boldsymbol{\eta}} \boldsymbol{y}\right) d\zeta, & \boldsymbol{\eta} \in \Omega_1^{\text{c}} \\ \displaystyle\int_{\grave{\zeta}(\boldsymbol{\eta})}^1 V_\zeta^2(\boldsymbol{\eta},\grave{\zeta}(\boldsymbol{\eta}),\zeta) \det\left(\nabla_{\boldsymbol{\eta}} \boldsymbol{y}\right) d\zeta, & \boldsymbol{\eta} \in \Omega_1^{\text{i}} \end{cases} \tag{4.8}$$

and recall the definition of the morphed images $\mathcal{I}_0$ and $\mathcal{I}_1$ defined in and following (4.2). With these definitions, the variational derivative of J_{of} with respect to σ_0 for fixed σ_1 is given compactly from (4.6) according to:

$$\frac{1}{2}\frac{\delta J_{\text{of}}}{\delta \sigma_0}(\sigma_0;\bar{\sigma}_0) = \int_{\Omega_0} \left[\sigma_0(I_0(\boldsymbol{\xi})) - \mathcal{I}_1(\boldsymbol{\xi})\right] \bar{\sigma}_0(I_0(\boldsymbol{\xi})) \mathcal{U}(\boldsymbol{\xi}) d\boldsymbol{\xi} + \int_{\Omega_1^{\text{i}}} \left[\sigma_0(I_0^\infty) - I_1(\boldsymbol{\eta})\right] \bar{\sigma}_0(I_0^\infty) \mathcal{V}(\boldsymbol{\eta}) d\boldsymbol{\eta}. \tag{4.9}$$

Now as with (4.1), (4.9) takes the form:

$$\begin{aligned}\frac{\delta J_{\mathrm{of}}}{\delta\sigma_0}(\sigma_0;\bar{\sigma}_0) &= 2\bar{\sigma}_0(I_0^\infty)\left[\int_{I_0(\boldsymbol{\xi})=I_0^\infty}[\sigma_0(I_0^\infty)-\mathcal{I}_1(\boldsymbol{\xi})]\mathcal{U}(\boldsymbol{\xi})d\boldsymbol{\xi}+\int_{\Omega_1^{\mathrm{i}}}[\sigma_0(I_0^\infty)-I_1(\boldsymbol{\eta})]\mathcal{V}(\boldsymbol{\eta})d\boldsymbol{\eta}\right]\\ &+ 2\sum_{\iota\in K_0\backslash\{I_0^\infty\}}\bar{\sigma}_0(\iota)\int_{I_0(\boldsymbol{\xi})=\iota}[\sigma_0(\iota)-\mathcal{I}_1(\boldsymbol{\xi})]\mathcal{U}(\boldsymbol{\xi})d\boldsymbol{\xi}\\ &+ 2\int_{\check{\iota}_0}^{\hat{\iota}_0}\bar{\sigma}_0(\iota)\left[\int_{I_0(\boldsymbol{\xi})=\iota,\nabla I_0(\boldsymbol{\xi})\neq 0}\frac{[\sigma_0(\iota)-\mathcal{I}_1(\boldsymbol{\xi})]\mathcal{U}(\boldsymbol{\xi})}{|\nabla I_0(\boldsymbol{\xi})|}d\boldsymbol{\xi}\right]d\iota\end{aligned} \tag{4.10}$$

Requiring this variational derivative to vanish for all perturbations $\bar{\sigma}_0$ leads to the following optimality condition for σ_0:

$$\sigma_0(\iota)=\begin{cases}\left[\displaystyle\int_{I_0(\boldsymbol{\xi})=\iota}\mathcal{I}_1(\boldsymbol{\xi})\mathcal{U}(\boldsymbol{\xi})d\boldsymbol{\xi}+\int_{\Omega_1^{\mathrm{i}}}I_1(\boldsymbol{\eta})\mathcal{V}(\boldsymbol{\eta})d\boldsymbol{\eta}\right]\Big/ \\ \qquad\left[\displaystyle\int_{I_0(\boldsymbol{\xi})=\iota}\mathcal{U}(\boldsymbol{\xi})d\boldsymbol{\xi}+\int_{\Omega_1^{\mathrm{i}}}\mathcal{V}(\boldsymbol{\eta})d\boldsymbol{\eta}\right], & \iota=I_0^\infty\\ \displaystyle\int_{I_0(\boldsymbol{\xi})=\iota}\mathcal{I}_1(\boldsymbol{\xi})\mathcal{U}(\boldsymbol{\xi})d\boldsymbol{\xi}\Big/\int_{I_0(\boldsymbol{\xi})=\iota}\mathcal{U}(\boldsymbol{\xi})d\boldsymbol{\xi}, & \iota\in K_0\backslash\{I_0^\infty\}\\ \displaystyle\int_{I_0(\boldsymbol{\xi})=\iota}\frac{\mathcal{I}_1(\boldsymbol{\xi})\mathcal{U}(\boldsymbol{\xi})d\boldsymbol{\xi}}{|\nabla I_0(\boldsymbol{\xi})|}\Big/\int_{I_0(\boldsymbol{\xi})=\iota}\frac{\mathcal{U}(\boldsymbol{\xi})d\boldsymbol{\xi}}{|\nabla I_0(\boldsymbol{\xi})|}, & \iota\in[\check{\iota}_0,\hat{\iota}_0]\backslash K_0\end{cases} \tag{4.11}$$

The optimality condition for σ_1 is given similarly by exchanging the subscripts 0 and 1, the variables $\boldsymbol{\xi}$ and $\boldsymbol{\eta}$, and the functions $\mathcal{U}(\boldsymbol{\xi})$ and $\mathcal{V}(\boldsymbol{\eta})$.

4.3 Interpretation of Optimality Conditions

To elucidate the meaning of (4.4) and (4.11), assume for simplicity that the optical flow $\boldsymbol{u}$ corresponds to a rigid transformation so that $\nabla\cdot\boldsymbol{u}=0$ holds and it follows with (3.14) and (3.15) that $U_\zeta=1$ and $V_\zeta=1$ hold. Furthermore, $\det(\nabla_{\boldsymbol{\xi}}\boldsymbol{x})=1$ and $\det(\nabla_{\boldsymbol{\eta}}\boldsymbol{y})=1$ hold. Hence, with (4.7) and (4.8) it follows that $\mathcal{U}=1$ and $\mathcal{V}=1$ hold. Thus, in this case (4.11) is identical to (4.4). Assume further now that I_0 and I_1 are both equal to one on their supports which are contained strictly within Ω_0^{c} and Ω_1^{c}, respectively. Assume also that σ_0 and σ_1 are initialized as the identity. Then according to (4.11), the average of $I_1(\boldsymbol{x}(\boldsymbol{\xi},1))$ over the support of $I_0(\boldsymbol{\xi})$ gives the value $\sigma_0(1)$. Similarly, the average of $I_0(\boldsymbol{y}(\boldsymbol{\eta},0))$ over the support of $I_1(\boldsymbol{\eta})$ gives the value $\sigma_1(1)$. With a perfect registration, $\sigma_0(1)=\sigma_1(1)=1$.

To illustrate the importance of scaling reciprocally, consider the two images shown in Fig. 3, for which the ideal registration transformation is the identity, i.e., these images are identical except that I_1 is noisy and I_0 is not. Specifically, $I_0=\chi_S$ and $I_1=I_1\chi_S$ hold, where the characteristic function χ_S of the set S satisfies $\chi_S=1$ on S and otherwise $\chi_S=0$. Assume now that no scaling is performed for I_1 so that $\sigma_1(\iota)=\iota$. Then, as explained above, $\sigma_0(1)$ is calculated as the average of I_1 over S. Specifically, $\sigma_0(I_0)$ remains a binary image while $\sigma_1(I_1)=I_1$ does not. Therefore, from (3.16) the intensity distribution $I^{(1)}(\boldsymbol{x},z)=\sigma_0(I_0(\boldsymbol{x}))[1-z]+I_1(\boldsymbol{x})z$ would drive a disturbance in $\boldsymbol{u}$ in the next update of the registration transformation. Assume now on the other hand, that no scaling is performed for I_0 so that $\sigma_0(\iota)=\iota$. Then since the average of I_0 on any subset of S is equal to one, the calculation of σ_1 gives $\sigma_1(I_1(\boldsymbol{x}))=I_0(\boldsymbol{x})$. Therefore, from (3.16) the intensity field $I^{(0)}(\boldsymbol{x},z)=I_0(\boldsymbol{x})$ preserves the identity transformation, unlike the case with scaling only on I_0. Thus, reciprocal scaling, as implemented in (3.9) and (3.10), is required for the registration result to be independent of the order in which images are taken.

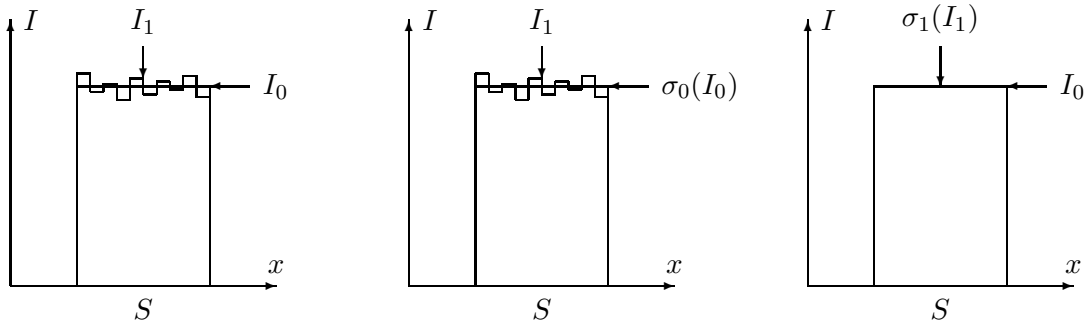

Figure 3: Scaling I_0 without scaling I_1 leaves $\sigma_0(I_0)$ a binary image. Scaling I_1 without scaling I_0 gives $\sigma_1(I_1) = I_0$. Thus, the result of nonreciprocal scaling depends upon the order in which images are taken.

This example also suggests that scaling can have an image smoothing effect, but to avoid that intensity resolution is lost ever more with each iteration of the minimization process, it is assumed that each scaling function is initialized to the identity just before its next update.

Although Fig. 3 illustrates the importance of reciprocal scaling in order that the registration be independent of image order, this order independence can only be shown in general for optical flow and not for finite displacements. For example, when the two given images can be matched using an affine registration and a rescaling, then $\boldsymbol{x}$ can be chosen so that both sides of (3.3) vanish. Otherwise, as shown in [10], unless $J_{\rm fd}$ contains a term $\mathcal{R}_{\rm fd}(\boldsymbol{y})$ penalizing $\boldsymbol{y}$ over Ω_1 exactly as $\boldsymbol{x}$ is penalized over Ω_0 in $\mathcal{R}_{\rm fd}(\boldsymbol{x})$, the registration result changes when the images are exchanged. On the other hand, order independence for optical flow can be seen by exchanging images and by replacing $I(\boldsymbol{x}, z)$, $\mathcal{I}(\boldsymbol{x}, z)$ and $\boldsymbol{u}(\boldsymbol{x})$ with $I(\boldsymbol{x}, 1-z)$, $\mathcal{I}(\boldsymbol{x}, 1-z)$ and $-\boldsymbol{u}(\boldsymbol{x})$ respectively and observing equality in (3.9), (3.10) and (3.18) after the transformation.

5 Regularization and Discretization of Scaling Functions

As can be seen from Figs. 4, 8 and 10 shown below, the formulas (4.4) and (4.11) derived above can lead to very irregular scaling functions, especially when the given images are noisy. In particular, the scaling functions are in general not monotone. In the case of very irregular scaling functions, Tikhonov regularization can be implemented by minimizing the following augmented cost functions:

$$J^{\nu}_{\rm fd}(\boldsymbol{x}, \sigma_0, \sigma_1) = J_{\rm fd}(\boldsymbol{x}, \sigma_0, \sigma_1) + \nu \int_0^1 |\sigma_0'(\iota)|^2 d\iota + \nu \int_0^1 |\sigma_1'(\iota)|^2 d\iota \quad (5.1)$$

$$J^{\nu}_{\rm of}(\boldsymbol{u}, I^{(0)}, I^{(1)}, \sigma_0, \sigma_1) = J_{\rm of}(\boldsymbol{u}, I^{(0)}, I^{(1)}, \sigma_0, \sigma_1) + \nu \int_0^1 |\sigma_0'(\iota)|^2 d\iota + \nu \int_0^1 |\sigma_1'(\iota)|^2 d\iota. \quad (5.2)$$

These estimations can be further simplified for the computation of scaling functions by expediently approximating the images as cellwise constant so that only the intensity ranges K_0 and K_1 are used. Under this assumption, let $\hat{\sigma}_0$ denote the function on the right side of (4.4) or (4.11), and let $\hat{\sigma}_1$ be given similarly. Then the minimizers of the augmented costs above are determined by:

$$\begin{cases} -\nu\sigma_0'' + \sigma_0 = \hat{\sigma}_0, & \iota \in (\check{\iota}_0, \hat{\iota}_0) \\ \sigma_0' = 0, & \iota = \check{\iota}_0, \hat{\iota}_0 \end{cases} \qquad \begin{cases} -\nu\sigma_1'' + \sigma_1 = \hat{\sigma}_1, & \iota \in (\check{\iota}_1, \hat{\iota}_1) \\ \sigma_1' = 0, & \iota = \check{\iota}_1, \hat{\iota}_1. \end{cases} \quad (5.3)$$

The functions $\hat{\sigma}_0$ and $\hat{\sigma}_1$ are now defined more precisely by formulating a discretization of the imaging domain. For this, let Q be divided into a grid of cells, each having dimensions $(h, \ldots, h, \tau)$, in the $x_1, \ldots, x_N$, and z directions, respectively, where $h = 2^{-p}$ and $\tau = 2^{-q}$ for integers p and q. Specifically, with the integer-component N-dimensional multi-indices

$\boldsymbol{i} = (i_1, \ldots, i_N)$, $\mathbf{0} = (0, \ldots, 0)$, and $\mathbf{1} = (1, \ldots, 1)$, define the cell corners by $(\mathbf{x}_{\boldsymbol{i}+1/2}, \mathrm{z}_{k+1/2}) = (\boldsymbol{i}h, k\tau)$, $\mathbf{0} \le \boldsymbol{i} \le 2^p \cdot \mathbf{1}$, $0 \le k \le 2^q$, and the cell centroids by $(\mathbf{x}_{\boldsymbol{i}}, \mathrm{z}_k) = ((\boldsymbol{i} - \frac{\mathbf{1}}{2})h, (k - \frac{1}{2})\tau)$, $\mathbf{1} \le \boldsymbol{i} \le 2^p \cdot \mathbf{1}$, $1 \le k \le 2^q$. Then, $I_{\boldsymbol{i},k}$ denotes the value of I at the cell centroid $(\mathbf{x}_{\boldsymbol{i}}, \mathrm{z}_k)$, and fractional indices are used for cell boundaries. Since the given images I_0 and I_1 are assumed to be cellwise constant, $I_0 = I_{0,\boldsymbol{i}}$ and $I_1 = I_{1,\boldsymbol{i}}$ hold within the $\boldsymbol{i}$th cell of Ω_0 and Ω_1 respectively.

With this discretization, the function $\hat{\sigma}_0$ is now defined explicitly as follows:

$$\hat{\sigma}_0(\iota) = \begin{cases} \left[\sum\limits_{I_{0,\boldsymbol{i}}=\iota} \mathcal{I}_{1,\boldsymbol{i}} \mathcal{U}_{\boldsymbol{i}} + \sum\limits_{\mathbf{x}_{\boldsymbol{i}} \in \Omega_1^{\mathrm{i}}} I_{1,\boldsymbol{i}} \mathcal{V}_{\boldsymbol{i}} \right] \Big/ \left[\int_{I_{0,\boldsymbol{i}}=\iota} \mathcal{U}_{\boldsymbol{i}} + \sum\limits_{\mathbf{x}_{\boldsymbol{i}} \in \Omega_1^{\mathrm{i}}} \mathcal{V}_{\boldsymbol{i}} \right], & \iota = I_0^{\infty} \\ \sum\limits_{I_{0,\boldsymbol{i}}=\iota} \mathcal{I}_{1,\boldsymbol{i}} \mathcal{U}_{\boldsymbol{i}} \Big/ \sum\limits_{I_{0,\boldsymbol{i}}=\iota} \mathcal{U}_{\boldsymbol{i}}, & \iota \in K_0 \backslash \{I_0^{\infty}\} \end{cases} \tag{5.4}$$

where:

$$\mathcal{I}_{1,\boldsymbol{i}} = \begin{cases} I_1(\boldsymbol{x}) \quad \boldsymbol{x} = \boldsymbol{x}(\mathbf{x}_{\boldsymbol{i}}) \text{ or } \boldsymbol{x}(\mathbf{x}_{\boldsymbol{i}}, 1) & \mathbf{x}_{\boldsymbol{i}} \in \Omega_0^{\mathrm{c}} \\ I_1^{\infty}, & \mathbf{x}_{\boldsymbol{i}} \in \Omega_0^{\mathrm{i}}. \end{cases} \tag{5.5}$$

The function $\hat{\sigma}_1$ is defined similar to (5.4) by exchanging the subscripts 0 and 1 and the functions $\mathcal{U}_i$ and $\mathcal{V}_i$. Also, $\mathcal{I}_{0,i}$ is defined similar to (5.5) by exchanging subscripts 0 and 1 and the transformations $\boldsymbol{x}(\mathbf{x}_i), \boldsymbol{x}(\mathbf{x}_i, 1)$ and $\boldsymbol{y}(\mathbf{x}_i), \boldsymbol{y}(\mathbf{x}_i, 0)$.

For finite displacements, (5.4) is understood with $\mathcal{U} = 1$ and $\mathcal{V} = 1$ to hold. For optical flow, $\mathcal{U}$ and $\mathcal{V}$ are obtained by integrating (3.7), (3.8), (3.14), (3.15), (4.7) and (4.8). As explained in [9], in order to obtain a sufficiently accurate intensity I at each cell centroid for the optical flow calculation, it is necessary to perform these trajectory integrations from each cell centroid both toward Ω_0 and toward Ω_1. These trajectory integrations are approximated using a Runge-Kutta method, where multilinear interpolation is used to obtain distributed values of the optical flow and its divergence. Also, optical flow derivatives are computed using central differences, with natural one-sided differences at the boundary, as are the metric terms, e.g., for $N = 2$, $\boldsymbol{e}_1 = (1, 0)$, $\boldsymbol{e}_2 = (0, 1)$:

$$\det\left[\nabla_{\boldsymbol{\xi}} \boldsymbol{x}(\mathbf{x}_{\boldsymbol{i}}, \zeta)\right] \approx \frac{1}{4h^2} \det \begin{bmatrix} x_1(\mathbf{x}_{\boldsymbol{i}+\boldsymbol{e}_1}, \zeta) - x_1(\mathbf{x}_{\boldsymbol{i}-\boldsymbol{e}_1}, \zeta) & x_1(\mathbf{x}_{\boldsymbol{i}+\boldsymbol{e}_2}, \zeta) - x_1(\mathbf{x}_{\boldsymbol{i}-\boldsymbol{e}_2}, \zeta) \\ x_2(\mathbf{x}_{\boldsymbol{i}+\boldsymbol{e}_1}, \zeta) - x_2(\mathbf{x}_{\boldsymbol{i}-\boldsymbol{e}_1}, \zeta) & x_2(\mathbf{x}_{\boldsymbol{i}+\boldsymbol{e}_2}, \zeta) - x_2(\mathbf{x}_{\boldsymbol{i}-\boldsymbol{e}_2}, \zeta) \end{bmatrix} \tag{5.6}$$

Thus, with $\hat{\sigma}_0$ and $\hat{\sigma}_1$ so determined from a given transformation and/or optical flow, the scaling functions are determined by (5.3), where derivatives are approximated by central differences in points ι in which values of $\hat{\sigma}_0$ and $\hat{\sigma}_1$ are given.

An investigated alternative to the optimize-then-discretize approach of (5.3) and (5.4) is the discretize-then-optimize approach of minimizing the unaugmented cost functions in (3.1) and (3.5) over a finite-dimensional basis for the scaling functions. Specifically, let the intervals $[\check{\iota}_0, \hat{\iota}_0]$ and $[\check{\iota}_1, \hat{\iota}_1]$ be divided into uniform grids of subintervals. Then let $\{\psi_k^{(0)}\}$ and $\{\psi_k^{(1)}\}$ be the linear splines (*hat*-functions) which form a basis for the piecewise linear continuous functions on the respective grids. In terms of these bases, the scaling functions take the form:

$$\sigma_0(\iota) = \sum_k \alpha_k^{(0)} \psi_k^{(0)}(\iota), \qquad \sigma_1(\iota) = \sum_k \alpha_k^{(1)} \psi_k^{(1)}(\iota) \tag{5.7}$$

where the coefficients $\{\alpha_k^{(0)}\}$ and $\{\alpha_k^{(1)}\}$ are determined by minimizing the unaugmented cost functions, i.e., $\mathcal{S}_{\mathrm{fd}}$ in (2.3) or $\mathcal{S}_{\mathrm{of}}$ in (4.6). This basis functions approach is compared to the Tikhonov regularization approach in Fig. 4 for the magnetic resonance images shown below in Fig. 6.

Note first in Fig. 4 that $\hat{\sigma}_0$ and $\hat{\sigma}_1$ are quite oscillatory. It is not *a priori* clear whether or not such raw scaling functions are inappropriate for measuring image similarity, but unregularized

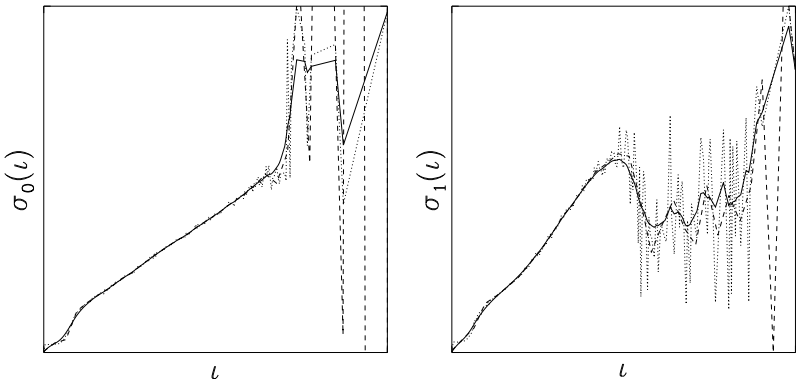

Figure 4: On the left are estimations of σ_0 and on the right are estimations of σ_1 for the registration example of Fig. 6. The dotted curves are $\hat{\sigma}_0$ and $\hat{\sigma}_1$ respectively. The dashed curves are scaling functions obtained by the basis functions approach. The solid curves are scaling functions obtained by the Tikhonov regularization approach.

scaling functions are found in practice to reduce excessively the discrimination capacity of the image similarity measure. Therefore, regularization is desirable. Secondly, note from Fig. 4 that the Tikhonov approach is clearly a regularization of the oscillatory functions, while the basis functions approach suffers extreme oscillations near large separations between points ι where values of $\hat{\sigma}_0$ or $\hat{\sigma}_1$ are given, i.e., between isolated peaks in the respective histograms. It may then be argued that the uniform grid for the basis functions should be adapted to match the signal strength of the image histograms. However, additional adaptive steps are as well circumvented by using the optimize-then-discretize approach. Thus, for the remainder of the paper, scaling functions are determined by (5.3) and (5.4).

The registration schemes for finite displacements and for optical flow which incorporate scaling functions in the image similarity measure can now be summarized algorithmically as follows.

- For finite displacements: set $\boldsymbol{x}(\boldsymbol{\xi}) = \boldsymbol{\xi}$ and continue the following until changes in $\boldsymbol{x}$ meet a convergence criterion:
  - solve (5.3) and (5.4) (with $\mathcal{U} = 1 = \mathcal{V}$) for σ_0 and the counterpart equations for σ_1,
  - solve one quasi-Newton step for the solution of (3.3) as explained in [10].
- For optical flow: set $\boldsymbol{u} = 0$ and continue the following until changes in $\boldsymbol{u}$ meet a convergence criterion:
  - perform the integrations (3.7), (3.8), (3.14), (3.15), (4.7) and (4.8),
  - solve (5.3) and (5.4) for σ_0 and the counterpart equations for σ_1,
  - solve (3.16) and (3.17) for $I^{(0)}$ and the counterpart equations for $I^{(1)}$, and use the results in (3.9) for I and (3.10) for $\mathcal{I}$,
  - solve (3.18) for the optical flow as explained in [10].

Note that for optical flow, the integrations (3.7), (3.8), (3.14) and (3.15) must be performed in order to compute the intensity, and the additional integrations (4.7) and (4.8) can be accumulated while performing the other integrations with very little extra cost. In any case, the work required to solve for the scaling functions is insignificant in relation to the work required to solve for the displacement field or for the optical flow.

6 Computational Results

In this final section, the algorithms summarized above are applied to a simple test case and to realistic examples taken from magnetic resonance imaging. As noted above, the cost for computing the scaling functions is quite small, and yet it is found here that the image similarity measured based upon scaling can provide a match between images with smaller errors than that obtained by the sum of squared differences alone.

The simple example shown in Fig. 5 is a two-dimensional elaboration of the example in

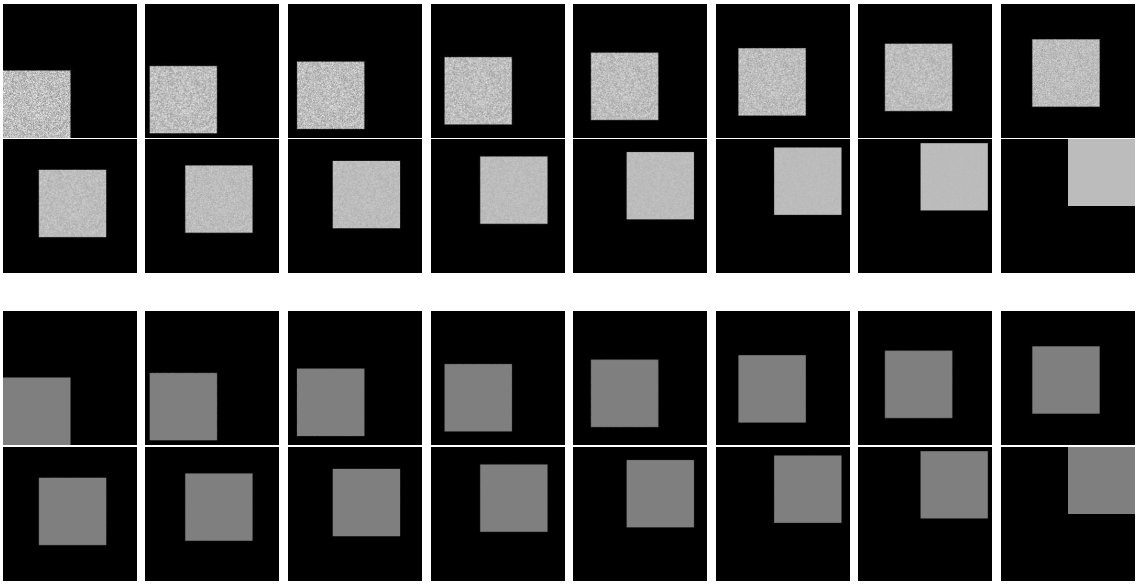

Figure 5: The two given images I_0 and I_1 are shown respectively in the extreme upper left and the extreme lower right. The intensities I and $\mathcal{I}$ are constructed for optical flow from $I^{(0)}$ and $I^{(1)}$ which are shown respectively in the top two and bottom two rows. Each sequence is to be read from left to right and from top to bottom.

Fig. 3, and it further illustrates the consequences of non-reciprocal scaling. The image shown in the extreme upper left is I_0 and the image shown in the extreme lower right is I_1. These two images clearly have quite different scalings and noise levels, as could be the case if they were measured by different modalities, but they are related by a simple translation. An optical flow has been used to interpolate between these images, and 16 slices of the intensity $I^{(0)}$ are shown in the top two rows, read from left to right and from top to bottom, while 16 slices of the intensity $I^{(1)}$ are shown in the bottom two rows, again read from left to right and from top to bottom. Recall that $I^{(0)}$ is computed by scaling only I_1 while $I^{(1)}$ is computed by scaling only I_0. The differences between $I^{(0)}$ and $I^{(1)}$ are analogous to those discussed in relation to Fig. 3, and the intensity I in (3.9) is used to compute the optical flow in (3.18) in order to permit reciprocal scaling and to avoid intensity variations, such as with $\mathcal{I}$ in (3.10), which result only from scaling differences as opposed to misregistration. On the other hand, once the optical flow has been computed, the intensity $\mathcal{I}$ is a more suitable interpolation than I. As discussed at the end of Section 4, both intensities I and $\mathcal{I}$ are simply reflected when the image order is reversed.

The example of Fig. 4 is now presented in more detail in Fig. 6. The images I_0 and I_1 shown in Fig. 6 are samples from a contrast enhanced image sequence in which there is very little motion while the patient allows the contrast agent to pass through the hand. Thus, the appeal of this example is that there is very little movement between the images and contrast agent appears at points of one image while not in the other. The finite displacement formulation has been used to register these images. In the first two rows of the figure, no scaling functions are used and the given images I_0 and I_1 are compared with the comparable morphs $\mathcal{I}_1$ and $\mathcal{I}_0$, respectively, while the registration errors $|I_i - \mathcal{I}_j|$ are shown in the rightmost column. Note

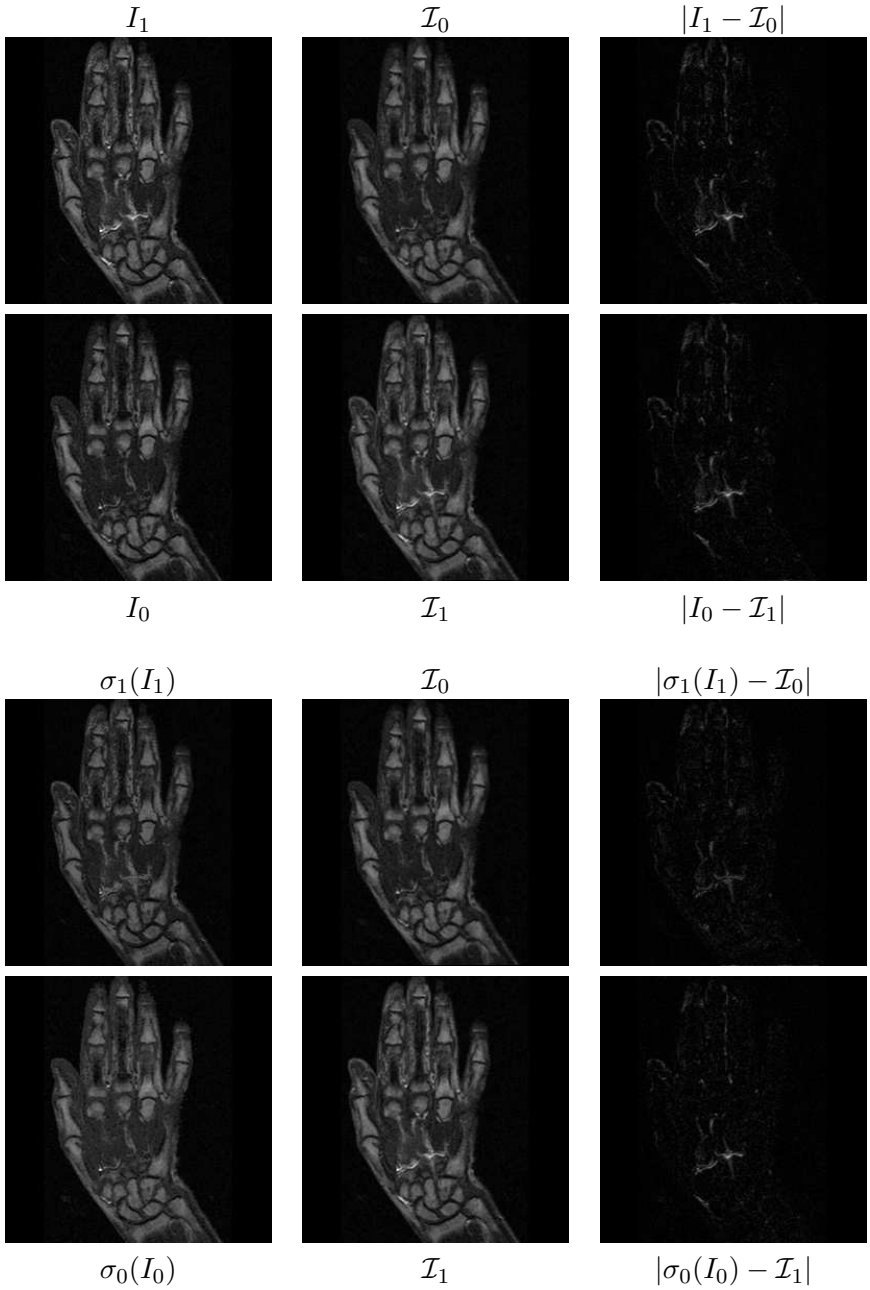

Figure 6: Images I_0 and I_1 are registered by finite displacements and with two similarity measures, with the sum of squared differences and with scaling functions, and the results are shown respectively in the top two rows and in the bottom two rows. The morphs $\mathcal{I}_j$, I_j toward I_i or $\sigma_i(I_i)$, are shown with errors $|I_i - \mathcal{I}_j|$ or $|I_i - \mathcal{I}_j|$.

that the largest differences between compared images are found where contrast agent appears in one image and not in the other. In the last two rows of the figure, scaling functions are used and the scaled images $\sigma_0(I_0)$ and $\sigma_1(I_1)$ are compared with the comparable morphs $\mathcal{I}_1$ and $\mathcal{I}_0$, respectively, while the registration errors $|\sigma_i(I_i) - \mathcal{I}_j|$ are shown in the rightmost column. Note that the smallest errors among compared images is found in $|\sigma_1(I_1) - \mathcal{I}_0|$. This can be understood since scaling functions are computed nonlocally from weighted averages over level sets. The high intensity regions of contrast agent in I_1 are isolated level sets and are therefore readily scaled down to the lower intensities of the corresponding regions of I_0. On the other hand, the corresponding regions in I_0 have intensities whose level sets are widely supported in I_0, and the isolated regions in question cannot be separated from their level sets in order to scale them up locally to the higher intensities in I_1. As a result, the errors found in $|\sigma_0(I_0) - \mathcal{I}_1|$ are

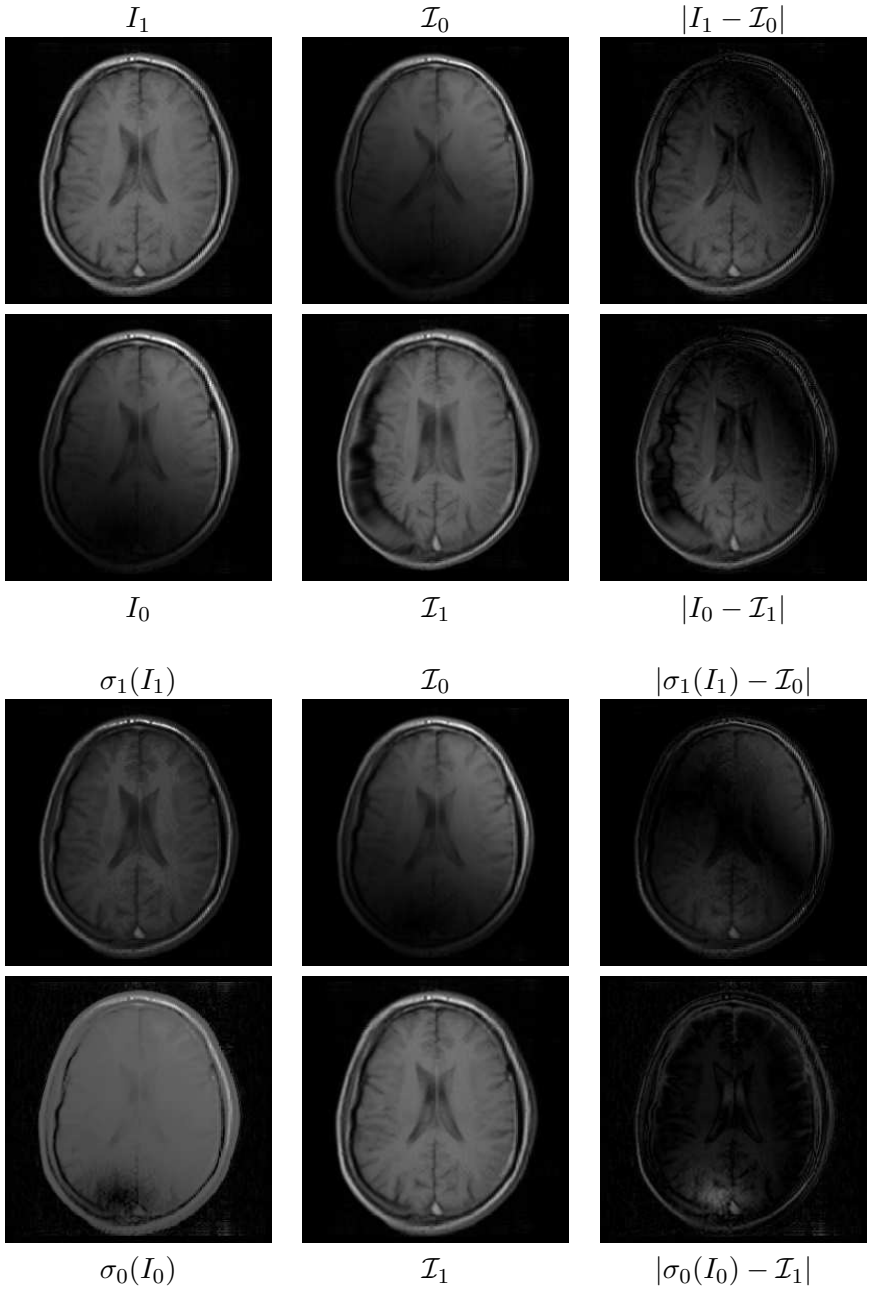

Figure 7: Images I_0 and I_1 are registered by finite displacements and with two similarity measures, with the sum of squared differences and with scaling functions, and the results are shown respectively in the top two rows and in the bottom two rows. The morphs $\mathcal{I}_j$, I_j toward I_i or $\sigma_i(I_i)$, are shown with errors $|I_i - \mathcal{I}_j|$ or $|I_i - \mathcal{I}_j|$.

not as small as in $|\sigma_1(I_1) - \mathcal{I}_0|$. Nevertheless, since all images and errors are displayed with the same intensity scale, it can be seen that the results with scaling functions provide smaller errors than those without scaling functions. Although smaller errors $|\sigma_i(I_i) - \mathcal{I}_j|$ do not necessarily imply a closer match, the deformation field computed with scaling functions for this example was found to be a trivial perturbation of the identity, which is consistent with the apparent absence of patient motion during the examination.

In the example shown in Fig. 7 the given image I_1 has been measured with a magnetic resonance coil which is large enough to provide uniform illumination while the given image I_0 has been measured with a small surface coil which leads to a nonuniform illumination [11]. As explained in [11], these images are measured immediately one after the other while the patient's head is restrained, and thus there is very little movement between the images. As with Fig. 6,

the finite displacement formulation has been used to register these images, and the display format in Fig. 7 is the same as in Fig. 6. Also, the scaling functions σ_0 and σ_1 are shown in Fig. 8. Since the all errors shown in the rightmost column of Fig. 7 are displayed with the same

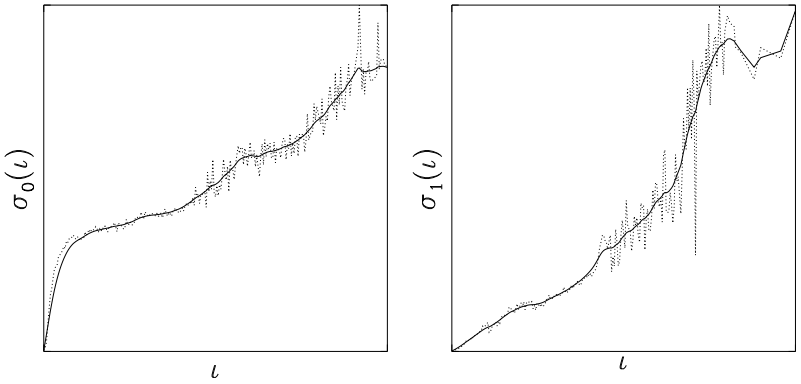

Figure 8: On the left are estimations of σ_0 and on the right are estimations of σ_1 for the registration example of Fig. 7. The dotted curves are $\hat{\sigma}_0$ and $\hat{\sigma}_1$ respectively. The solid curves are scaling functions obtained by Tikhonov regularization.

greyscale, it is readily seen that the results with scaling functions provide smaller errors than those without scaling functions. Furthermore, it may be concluded that the results with scaling functions are more accurate since the nonuniform illumination has led to an obvious distortion in the morph produced using only the sum of squared differences, while no such distortion appears in the results with scaling functions. Note that the scaling functions are designed to accomplish contrast modulation, as opposed to inhomogeneity correction; thus, the success of the new similarity measure for the example of Fig. 7 must be understood on the basis that much contrast, indeed resolution, has been lost in the scaled images, particularly $\sigma_0(I_0)$, and the low resolution images are better matched than the nonuniformly illluminated images.

The last two examples were also chosen for the absence of large displacements so that image similarity would be the focus. In the example of Fig. 9, respiratory motion accompanies the sudden and widespread appearance of contrast agent, particularly in the kidneys, and it is required to interpolate between the two given images shown respectively on the left and on the right of the figure. The other images in the figure are samples taken from an interpolation computed by optical flow. Note that in the images toward the right, the kidneys are higher and brighter than they are in the images toward the left. The computed scaling functions are shown in Fig. 10. Note from Fig. 5 that neither of the intensities $I^{(0)}$ or $I^{(1)}$ are an adequate interpolation between images of interest in this work. Nevertheless, the interpolated images of Fig. 9, given by $\mathcal{I}$ in (3.10), are well suited to the interpolation problem. The two end images in Fig. 9 are actually one pair taken from a lengthy temporal sequence in which temporal resolution is low enough for the raw sequence to be quite jerky but high enough to permit a smooth interpolation which facilitates the medical examination. The raw and interpolated films can be viewed by downloading them respectively from:

`http://math.uni-graz.at/invcon/medimage/respfilm1.mpg`
`http://math.uni-graz.at/invcon/medimage/respfilm2.mpg`.

References

[1] R.A. Adams, *Sobolev Spaces*, Academic Press, New York, 1975.

[2] V. Caselles and L. Garrido, *A contrast invariant approach to motion estimation*, Scale Space 2005, Hofgeismar, Germany, 7-9 April, 2005.

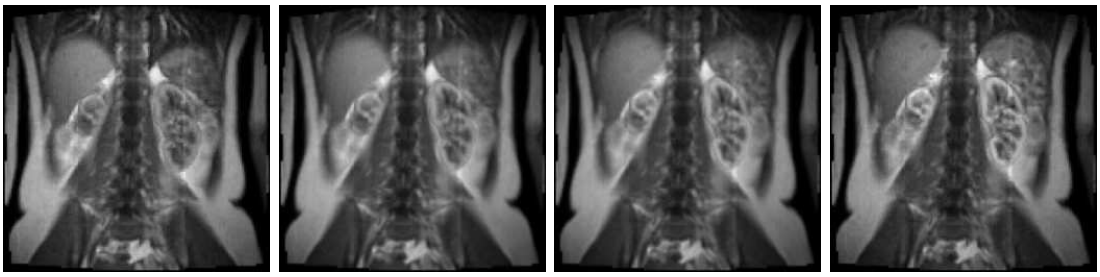

Figure 9: The two given images I_0 and I_1 are shown respectively on the left and on the right. The images in between have been interpolated by optical flow using (3.10).

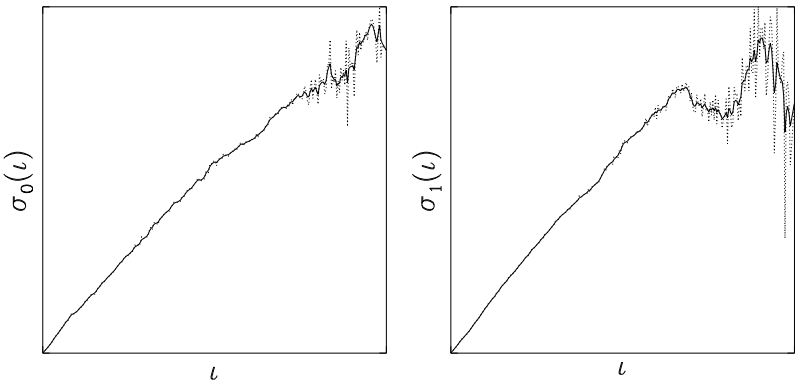

Figure 10: On the left are estimations of σ_0 and on the right are estimations of σ_1 for the registration example of Fig. 9. The dotted curves are $\hat{\sigma}_0$ and $\hat{\sigma}_1$ respectively. The solid curves are scaling functions obtained by Tikhonov regularization.

[3] M. Droske and W. Ring, *A Mumford-Shah Level-Set Approach for Geometric Image Registration*, Preprint Series DFB-SPP 1114, Preprint 99, April 2005.

[4] M. Droske and M. Rumpf, *A Variational Approach to Non-Rigid Morphological Registration*, SIAM J. Appl. Math., Vol. 64, No. 2, pp. 668–687, 2004.

[5] L.C. Evans and R.F. Gariepy, *Measure Theory and Fine Properties of Functions*, CRC Press, Boca Raton, 1992.

[6] B. Fischer and J. Modersitzki, *Curvature Based Image Registration*, J. Math. Imaging and Vision 18, pp. 81–85, 2003.

[7] S. Henn, *A Multigrid Method for a Fourth-Order Diffusion Euation with Application to Image Processing*, SIAM J. Sci. Comput. (SISC), Vol. 27, No. 3, pp. 831–849, 2005.

[8] B.K.P. Horn and B.G. Schunck, *Determining Optical Flow*, Artif. Intell., Vol. 23, pp. 185 – 203, 1981.

[9] S.L. Keeling and W. Ring, *Medical Image Registration and Interpolation by Optical Flow with Maximal Rigidity*, J. Math. Imag. Vision, Vol. 23, No. 1, pp. 47–65, July 2005.

[10] S.L. Keeling, *Geometric Multigrid for Generalized Rigid and Affine Image Registration and Interpolation*, to appear in J. Math. Imag. Vision.

[11] S.L. Keeling and R. Bammer, *A Variational Approach to Magnetic Resonance Coil Sensitivity Estimation*, Appl. Math. Comp., Vol. 158, pp. 359–388, 2004.

[12] F. Maes, A. Collignon, D. Vandermeulen, G. Marchal and P. Suetens, *Multimodality Image Registration by Maximization of Mutual Information*, IEEE Trans. Med. Imaging, Vol. 16, pp. 187–109, 1997.

[13] J. Modersitzki, *Numerical Methods for Image Registration*, Oxford University Press, 2004.

[14] D. Rueckert, B. Clarkson, D.L.G. Hill and D.J. Hawkes, *Non-rigid Registration using Higher-Order Mutual Information*, Medical Imaging 2000: Image Processing, K. M. Hanson, ed., Proceedings of SPIE, Vol. 3979, pp. 438–447, 2000.

[15] J.-P. Thirion, *Image Matching as a Diffusion Process: An Analogy with Maxwell's Demons*, Medical Image Analysis, Vol. 2, No. 3, pp. 243 – 260, 1998.

[16] P.A. Viola, *Alignment by Maximization of Mutual Information.*, Ph.D. thesis, Massachusetts Institute of Technology, 1995.

[17] J. Weickert, A. Bruhn, N. Papenberg and T. Brox, *Variational Optical Flow Computation: From Continuous Models to Algorithms*, Otmar Scherzer (ed): Mathematical Method for Registration and Applications to Medical Imaging, Mathematics in Industry, Springer, Vol. 10, 2006.